

Threshold stress intensity factor and crack growth rate prediction under mixed-mode loading

Yongming Liu, Sankaran Mahadevan *

Vanderbilt University, Nashville, TN 37235, USA

Received 16 February 2006; received in revised form 2 June 2006; accepted 9 June 2006

Available online 8 August 2006

Abstract

A new mixed-mode threshold stress intensity factor is developed using a critical plane-based multiaxial fatigue theory and the Kitagawa diagram. The proposed method is a nominal approach since the fatigue damage is evaluated using remote stresses acting on a cracked component rather than stresses near the crack tip. An equivalent stress intensity factor defined on the critical plane is proposed to predict the fatigue crack growth rate under mixed-mode loading. A major advantage is the applicability of the proposed model to many different materials, which experience either shear or tensile dominated crack growth. The proposed model is also capable to nonproportional fatigue loading since the critical plane explicitly considers the influence of the load path. The predictions of the proposed fatigue crack growth model under constant amplitude loading are compared with a wide range of fatigue results in the literature. Excellent agreements between experimental data and model predictions are observed.

© 2006 Published by Elsevier Ltd.

Keywords: Fatigue crack; Threshold stress intensity factor; Crack growth; Mixed-mode loading

1. Introduction

The investigation of fatigue crack behavior using fracture mechanics has been largely focused on mode I loading [1]. However, engineering components or structures are often subjected to both normal and shear loading (modes II and III). This type of fatigue problem is usually referred to either as the multiaxial fatigue problem for classical fatigue analysis ($S-N$ or $e-N$ curve approach) or the mixed-mode fatigue crack problem within the context of fracture mechanics. Several reviews of existing multiaxial fatigue models [2,3] and mixed-mode fatigue crack growth models [4,5] are available in the literature. A comprehensive review and comparison of different models is not the objective of the current study and thus only a few of them are briefly described below.

For the multiaxial fatigue models using the $S-N$ ($e-N$) curve approach, the critical plane-based models have been gaining popularity due to their success in accurately predicting lives [2]. The development of the critical

* Corresponding author. Tel.: +1 615 322 3040; fax: +1 615 322 3365.

E-mail address: Sankaran.Mahadevan@vanderbilt.edu (S. Mahadevan).

plane approach is based on the observations that the fatigue crack nucleated along certain planes in the material. The planes are named “critical plane” and the stress (strain) components on it are used for fatigue analysis [3]. Liu and Mahadevan [6] examined various critical plane-based models and grouped them into two categories based on their underlying failure mechanisms. A number of the critical plane approaches are for the shear failure mode and some others are for the tensile failure mode. It has been found that the methods based on one failure mode perform poorly for the fatigue modeling of the other failure mode [7,8]. Jiang [9] proposed an incremental critical plane-based model. The Jiang model can deal with tensile cracking, shear cracking, and mixed cracking behavior. Recent work by Jiang and Feng [10] and Feng et al. [11] has extended the application of the Jiang multiaxial fatigue criterion to predicting general crack growth. As the Jiang model used plastic strain energy as the major measure of the fatigue damage, the model is only applicable to ductile materials.

For the mixed-mode fatigue crack models, a similar trend comparable with those of the multiaxial fatigue models can be found in the literature. A number of existing models assume that the tensile crack growth dominates during the fatigue crack propagation. The maximum tangential stress (MTS) criterion proposed by Erdogan and Sih [12] and the maximum tangential strain (MTSN) criterion proposed by Chambers et al. [13] are two typical models using the tensile failure mode assumption. Yan et al. [14] used an equivalent stress intensity factor defined on the maximum tangential stress plane, which also assumed the tensile failure mode. Many other models based on energy concepts, such as the energy release rate model [15], the strain energy density model [16] and the dilatational strain energy density model [17], can be also deemed as variations of a tensile failure-based model similar to the MTS criterion [18]. Compared with a large number of models based on the tensile failure mode, relatively few models based on the shear failure mode are available in the literature. Otsuka et al. [19] observed Mode II crack growth in ductile steels and stated that fatigue cracks can either grow along the maximum tangential stress plane (mode I) or along the maximum shear stress plane (mode II). A similar approach for the crack growth under static loading has been proposed by Chao and Liu [18], in which the MTS criterion and the MSS (maximum shear stress) criterion are combined together to predict the crack growth. Socie et al. [20] proposed an equivalent strain intensity factor for the near threshold small crack growth, which is defined on the maximum shear strain plane. A similar approach was also proposed by Reddy and Fatemi [21].

It is well known that models based on the tensile failure mode work well for brittle materials. For ductile materials, both mode I and mode II cracks could occur and the models based on a single failure mechanism cannot give a satisfactory prediction [4,18]. For mixed-mode fatigue crack growth, it has been reported that the crack could change the growth mode depending on the applied loading amplitude [22]. Gao et al. [22] observed that the near threshold crack growth is shear-mode and the crack branches to tensile-mode when the applied mixed-mode loading is gradually increased. This type of observation indicates that no single model based on a specific failure mechanism can be applied to the whole regime of the fatigue crack growth, i.e., from near-threshold crack growth to long crack growth, since the underlying failure mechanisms could be different.

For the fatigue problem under multiaxial loading, the nonproportionality of the applied loading is another important factor affecting the fatigue life. The effects of different loading paths on the fatigue crack initiation life have been studied by previous researchers [6,23–25]. For mixed-mode fatigue crack propagation, several studies have focused on the nonproportionality effect [1,4,26]. Feng et al. [26] observed different crack growth behavior under different loading paths with identical loading magnitude in the axial and the torsional directions and stated that many models using applied stress intensity range or *J-integral* range are not capable under this situation as they produce identical predictions under different loading paths. A reasonable model for mixed-mode fatigue crack growth should consider the loading path effects.

In this study, a new model for mixed-mode threshold stress intensity factor and growth rate prediction is proposed. The method is a nominal approach since it is developed using remote stresses rather than stresses near the crack tip. Two major advantages of the proposed model are that it can automatically adapt for different failure mechanisms and that it considers the loading path effects. A multiaxial fatigue limit criterion proposed earlier by the authors [27] is extended to develop a threshold stress intensity factor criterion using the Kitagawa diagram [28]. Following this, an equivalent stress intensity factor is proposed for the crack growth rate prediction. The predictions of the proposed fatigue damage model under constant amplitude loading are compared with a wide range of experimental fatigue results in the literature.

2. Proposed model for mixed-mode fatigue

2.1. Multiaxial fatigue limit criterion

A stress-based approach is commonly used for high-cycle fatigue analysis. The stress-based approaches can be divided into four groups based on empirical equivalent stress, stress invariants, average stress and critical plane stress [2]. Liu and Mahadevan [27] proposed a critical-plane based model for multiaxial fatigue damage modeling and validated the model using bending-torsional fatigue experimental data. Different from most existing critical plane-based models, the proposed method does not rely on the cracking mechanisms, such as the crack growth orientations [27]. The critical plane in the proposed model is only a material plane on which the stress/strain components are used to analyze the fatigue damage of materials. It arises from the idea of mathematical dimensional reduction rather than the physical cracking observations. Even without knowing the cracking mechanisms, the proposed method can still be applied. This is one of the advantages of the proposed method. For example, this feature makes it possible to be applied to both metallic and composite materials, even through the cracking mechanism for the two materials are fundamentally different [29].

The plane experiencing maximum normal stress amplitude is first identified in the proposed method. The angle between the critical plane and the maximum normal stress amplitude plane is γ , which depends on different materials. A detailed derivation and explanation of the model can be found in Liu and Mahadevan [27]. Only the results are shown here. The general fatigue limit criterion under multiaxial loading is expressed as

$$\sqrt{\left(\frac{\sigma_c}{f_{-1}}\right)^2 + \left(\frac{\tau_c}{t_{-1}}\right)^2} + A\left(\frac{\sigma_H}{f_{-1}}\right)^2 = B \quad (1)$$

where σ_c and τ_c are the normal stress amplitude and shear stress amplitude acting on the critical plane, respectively. σ_H is the hydrostatics stress amplitude. A and B are material parameters which can be determined by uniaxial and torsional fatigue limits. Material parameters A , B and γ are listed in Table 1. The material parameter $s = \frac{t_{-1}}{f_{-1}}$ is related to the material ductility and affects the critical plane orientation. For brittle materials, the critical plane is close to the maximum normal stress amplitude plane. For ductile materials, the critical plane is close to the maximum shear stress amplitude plane. Thus this model can automatically adapt for different failure modes, i.e., tensile or shear dominated failure. The model is load path-dependent since different loading paths result in different critical plane orientations and thus different fatigue life prediction.

Liu et al. [30] modified the above criterion to be applicable to a general 3D stress condition. Out-of plane shear stress component is included in the criterion and Eq. (1) is rewritten as

$$\sqrt{\left(\frac{\sigma_{c(1)}}{f_{-1}}\right)^2 + \left(\frac{\tau_{c(2)}}{t_{-1}}\right)^2 + \left(\frac{\tau_{c(3)}}{t_{-1}}\right)^2} + A\left(\frac{\sigma_H}{f_{-1}}\right)^2 = B \quad (2)$$

where the subscripts (1), (2), (3) of σ_c and τ_c indicate the directions of the stress amplitude as shown in Fig. 1. For the axial-torsional loading, one component of shear stress amplitude reduces to zero, and Eq. (2) reduces to Eq. (1).

Table 1
Material parameters for fatigue limit criterion

Material property	$s = \frac{t_{-1}}{f_{-1}} \leq 1$	$s = \frac{t_{-1}}{f_{-1}} > 1$
γ	$\cos(2\gamma) = \frac{-2 + \sqrt{4 - 4(1/s^2 - 3)(5 - 1/s^2 - 4s^2)}}{2(5 - 1/s^2 - 4s^2)}$	$\gamma = 0$
A	$A = 0$	$A = 9(s^2 - 1)$
B	$B = [\cos^2(2\gamma)s^2 + \sin^2(2\gamma)]^{\frac{1}{2}}$	$B = s$

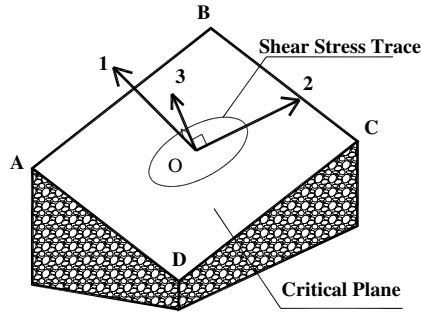


Fig. 1. Critical plane definition.

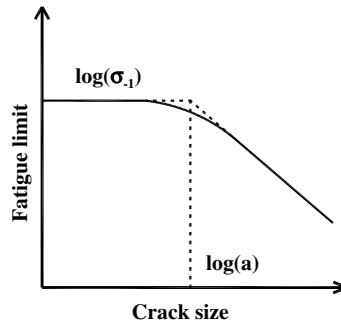


Fig. 2. Schematic representation of Kitagawa diagram for fatigue limits and threshold stress intensity factor.

2.2. Fatigue limit and threshold stress intensity factor

The concept of fatigue limit is traditionally used within the fatigue resistance design approach, which defines a loading criterion under which no macroscopic crack will form. The concept of threshold stress intensity factor is often used within the damage tolerant design approach, which defines a loading criterion under which the cracks will not grow significantly [31]. A link between the fatigue limit and the threshold stress intensity factor was proposed by Kitagawa and Takahashi [28]. The fatigue limit against the crack size using the Kitagawa diagram is shown in Fig. 2. According to the well-known El Haddad model [32], the fatigue limit can be expressed using the threshold stress intensity factor and a fictional crack length *a*. The crack length *a* represents the intersection of the smooth specimen fatigue limit and the linear elastic fracture mechanics (LEFM) threshold stress intensity factor, i.e.,

$$f_{-1} = \frac{K_{I,th}}{\sqrt{\pi a}} \tag{3}$$

where $K_{I,th}$ is the threshold stress intensity factor for mode I loading. A similar formula can be also expressed for mode II (or III) loading

$$t_{-1} = \frac{K_{II,th}}{\sqrt{\pi a}} \quad \text{or} \quad \left(t_{-1} = \frac{K_{III,th}}{\sqrt{\pi a}} \right) \tag{4}$$

where $K_{II,th}$ and $K_{III,th}$ are the threshold stress intensity factors for mode II and mode III loading, respectively.

2.3. Mixed-mode I + II threshold stress intensity factor

As shown in the last section, the Kitagawa diagram links the fatigue behavior of cracked and noncracked material together. Using this concept, it is easy to extend the multiaxial fatigue limit criterion in Section 2.1 to a mixed-mode threshold stress intensity factor criterion, as derived below.

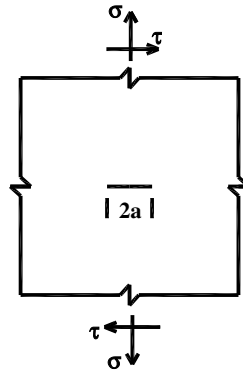


Fig. 3. Center crack in a infinite plate under remote multiaxial stress.

To facilitate the discussion, first consider a simple problem as shown in Fig. 3. An infinite plate is under remote tensile stress and shear stress, which has a centered crack of length $2a$. This results in a mixed-mode I and II condition near the crack tip. Suppose the remote tensile stress has a range of σ with zero stress ratio and the remote shear stress has a range of τ with zero stress ratio.

The range of the mode I stress intensity factor is

$$K_I = \sigma\sqrt{\pi a} \tag{5}$$

The range of the mode II stress intensity factor is

$$K_{II} = \tau\sqrt{\pi a} \tag{6}$$

Substituting Eqs. (3)–(6) into Eq. (1) and Table 1, we obtain

$$\sqrt{\left(\frac{k_1}{K_{I,th}}\right)^2 + \left(\frac{k_2}{K_{II,th}}\right)^2} + A\left(\frac{k^H}{K_{I,th}}\right)^2 = B \tag{7}$$

where k_1, k_2 and k^H are loading-related parameters with the same units as stress intensity factor. For proportional multiaxial loading, they can be expressed as

$$\begin{cases} k_1 = \frac{K_I}{2}(1 + \cos 2\alpha) + K_{II} \sin 2\alpha \\ k_2 = -\frac{K_I}{2} \sin 2\alpha + K_{II} \cos 2\alpha \\ k^H = \frac{K_I}{3} \end{cases} \tag{8}$$

where α is the critical plane orientation. It can be expressed as

$$\alpha = \beta + \gamma \tag{9}$$

where β is the maximum normal stress amplitude plane orientation at the far field. For proportional loading, $\beta = \frac{1}{2} \tan^{-1} \left(\frac{2K_{II}}{K_I} \right)$. A schematic representation of the critical plane orientation is shown in Fig. 4. Fig. 4

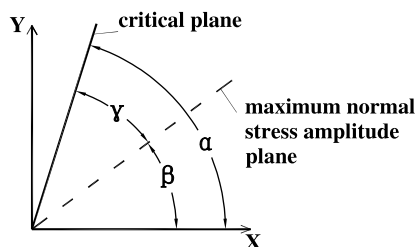


Fig. 4. Orientation of critical plane and maximum normal stress plane.

illustrates the critical plane orientation and its relationship with the original coordinate and the maximum normal stress amplitude plane. In the proposed method, the critical plane depends on the applied loading (i.e., the maximum normal stress amplitude plane β) and the material properties (i.e., the angle between the critical plane and the maximum normal stress amplitude plane γ). The orientation α of the critical plane is the summation of both β and γ .

For general nonproportional loading, the axial loading and the torsional loading may not reach the maxima simultaneously. Numerical search is required to find the value of β , k_1 and k_2 [30]. γ has been defined in Table 1 earlier. Note that s in Table 1 is redefined using the threshold stress intensity factor under mode I and mode II loading as $s = \frac{K_{II,th}}{K_{I,th}}$. Eqs. (7)–(9) together with the material parameters defined in Table 1 are used for threshold stress intensity factor prediction under general mixed-mode loading.

In Eq. (8), k_1 and k_2 are loading-related parameters with the same units as the stress intensity factor. However, they are not the same as those defined in the fracture mechanics for kinked cracks [33]. The equivalent stress intensities of kinked crack are obtained using the stress field near the crack tip. The proposed parameters are obtained using the remote stress transformation and thus we name the proposed model as a nominal approach.

Similar to Liu and Mahadevan [30], the ratio of mode II and mode I threshold stress intensity factor $s = \frac{K_{II,th}}{K_{I,th}}$ is related two different material failure mechanisms. A larger value of s ($s \geq 1$) indicates tension-dominated failure and smaller s ($s \leq \frac{1}{\sqrt{3}}$) indicates shear-dominated failure. If the value of s is known (based on uniaxial and pure torsional fatigue tests), the proposed model can automatically adapt for different failure mechanisms.

2.4. Mixed-mode I + II fatigue crack growth

After developing the threshold stress intensity factor criterion as above, the methodology for fatigue crack growth rate prediction is relatively easy. Note that the threshold stress intensity factor is often related to the stress intensity at a very low crack growth rate ($\frac{da}{dN} < 10^{-8}$ – 10^{-7} mm/cycle). Eq. (7) can be rewritten as

$$\frac{1}{B} \sqrt{(k_1)^2 + \left(\frac{k_2}{s}\right)^2 + A(k^H)^2} = K_{I,th} \tag{10}$$

The left side of Eq. (10) can be treated as the equivalent stress intensity. It can be used to correlate with the crack growth rate using the mode I crack growth curve. For prediction corresponding to a general crack growth rate da/dN , the threshold stress intensity factors ($K_{I,th}$ and $K_{II,th}$) may be replaced by the stress intensity coefficients at the specific crack growth rate ($K_{I,da/dn}$ and $K_{II,da/dn}$). In the proposed mixed-mode crack growth model, stress intensity coefficients at the specific crack growth rates are considered as equivalent stress intensity factor for mixed-mode case. Then the mixed-mode crack growth model is expressed as

$$K_{mixed,eq} = \frac{1}{B} \sqrt{(k_1)^2 + \left(\frac{k_2}{s}\right)^2 + A(k^H)^2} = K_{I,da/dn} = f\left(\frac{da}{dN}\right) \tag{11}$$

where $f\left(\frac{da}{dN}\right)$ is the crack growth curve obtained under mode I loading. The quantity s in Table 1 is redefined as $s = \frac{K_{II,da/dN}}{K_{I,da/dN}}$. Eq. (11) has no closed-form solution. In practical calculation, a trial and error method can be used to find $\frac{da}{dN}$. For high cycle fatigue problem, $K_{II,da/dN}$ and $K_{I,da/dN}$ take initial values as $K_{II,th}$ and $K_{I,th}$, respectively. It is found that usually a few iterations are enough to make N_f converge. Eq. (11) together with the parameters in Table 1 may be used for fatigue crack growth rate prediction under mixed-mode loading.

2.5. Mixed-mode I + III and I + II + III crack

The above derivation is for mixed-mode I + II loading. Similar results can be obtained for mixed-mode I + III loading. For isotropic materials, no difference is obtained for fatigue limit for in-plane shear stress

or out-of-plane shear stress. These two different loadings result in mode II and mode III stress intensity factors if the frictional crack is included. Similar to Eq. (6), the mode III stress intensity factor can be expressed as

$$K_{III} = \tau\sqrt{\pi a} \quad (12)$$

a refers to the crack depth under the mixed-mode I + III loading and refers to the crack length (surface crack) under the mixed-mode I + II loading. The experimental verification of mixed-mode I + II conditions and mixed-mode I + III conditions shown in the next section recognizes the above definition. Following the same procedure as described in Sections 2.2 and 2.3, the mixed-mode I + III threshold stress intensity factor and growth rate model can be also developed. They are almost same with those for mode I + II except all the mode II components are replaced by mode III components, i.e., K_{II} , $K_{II,th}$ and $K_{II,da/dN}$ are replaced by K_{III} , $K_{III,th}$ and $K_{III,da/dN}$, respectively

$$\sqrt{\left(\frac{k_1}{K_{I,th}}\right)^2 + \left(\frac{k_3}{K_{III,th}}\right)^2 + A\left(\frac{k^H}{K_{I,th}}\right)^2} = B \quad (13)$$

$$K_{mixed,eq} = \frac{1}{B} \sqrt{(k_1)^2 + \left(\frac{k_3}{s}\right)^2 + A(k^H)^2} = K_{I,da/dN} = f\left(\frac{da}{dN}\right) \quad (14)$$

If the material is under remote tensile stress, in-plane and out-plane shear stress, it results in mixed-mode I + II + III loading on the crack. Compared with mode I + II and mode I + III loading, the problem is more difficult, especially when none of these stress components is proportional. Eq. (2) is used for general mixed-mode loading. Following the same procedure for the mixed-mode I + II case, the formulas for general mixed-mode I + II + III loading are derived as

$$\sqrt{\left(\frac{k_1}{K_{I,th}}\right)^2 + \left(\frac{k_2}{K_{II,th}}\right)^2 + \left(\frac{k_3}{K_{III,th}}\right)^2 + A\left(\frac{k^H}{K_{I,th}}\right)^2} = B \quad (15)$$

$$K_{mixed,eq} = \frac{1}{B} \sqrt{(k_1)^2 + \left(\frac{k_2}{s}\right)^2 + \left(\frac{k_3}{s}\right)^2 + A(k^H)^2} = K_{I,da/dN} = f\left(\frac{da}{dN}\right) \quad (16)$$

3. Experimental validation

3.1. Comparisons of the threshold stress intensity factor

Eight sets of fatigue experimental data available in the literature are employed in this section, and are listed in Table 2. The predicted thresholds and the experimental observations are plotted in Fig. 5. In Fig. 5, the x -axis and the y -axis are the applied stress intensity ranges for mode I and mode II (or mode III), respectively. All values are normalized using the mode I threshold stress intensity factor. For comparisons, the predictions using the MTS, the maximum strain energy release rate and the minimum strain energy density are also plotted.

Table 2
Experimental threshold data used for model validation

Material name	References	Loading case	$K_{I,th}$ (MPa m ^{1/2})	$s = K_{II,th}/K_{I,th}$
6061Al	[34]	I + II	3.9	0.55
7075-T6 Aluminum alloy	[35]	I + II	1.6	0.64
316 Stainless steel	[22]	I + II	5.81	0.7
Aluminum alloy	[36]	I + II	2.75	0.83
2017-T3 Aluminum alloy	[35]	I + II	1.6	0.9
Mild steel	[37]	I + III	6.6	1.1
2024Al	[38]	I + II	3.9	1.46
SiCp/2024Al composite	[38]	I + II	4.8	1.79

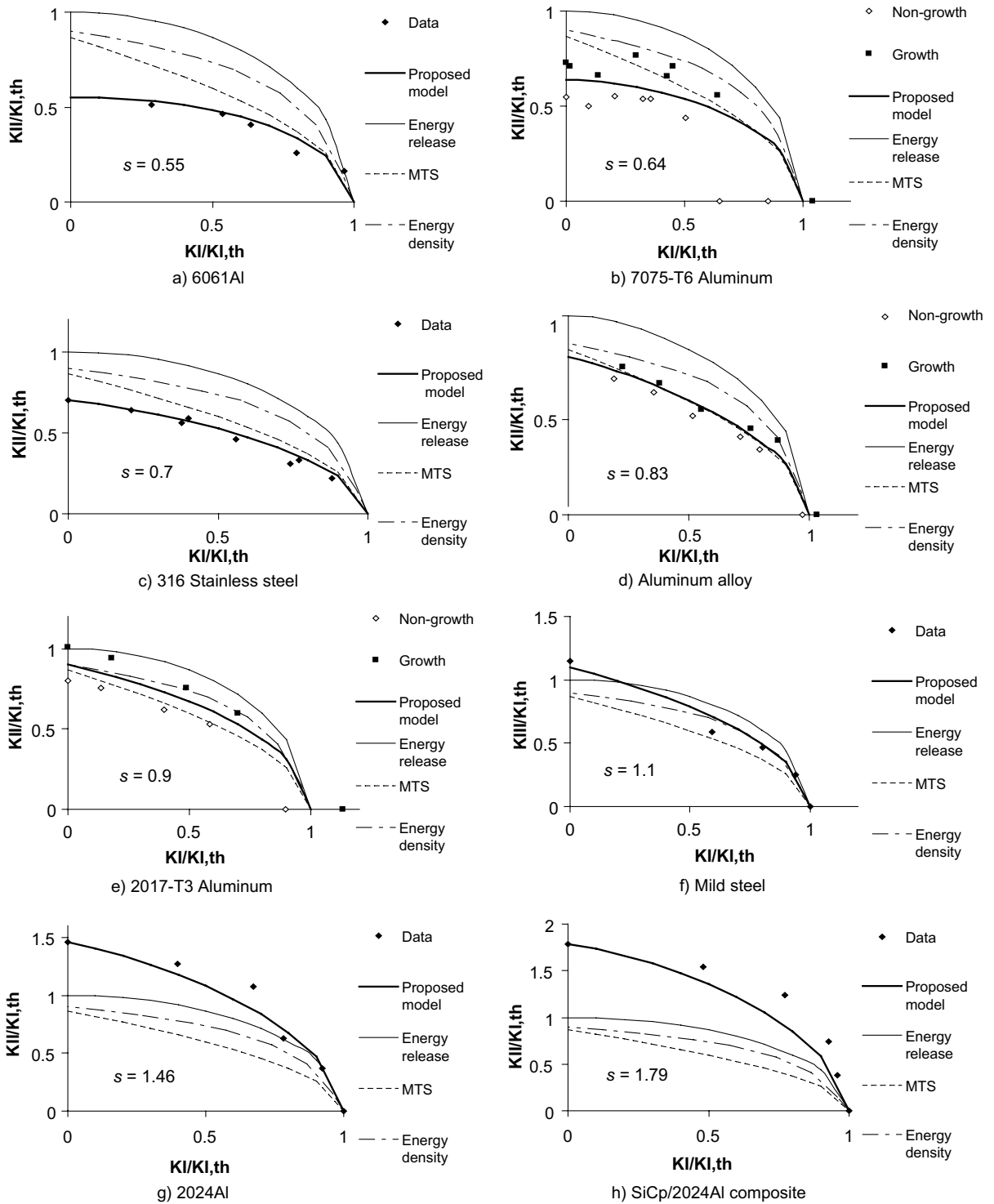


Fig. 5. Comparisons of predicted and experimental threshold stress intensity factors.

Two different formats of experimental data are collected. Several materials (6061Al, 316 stainless steel, mild steel, 2024Al, SiCp/2024Al composite) used the threshold stress intensity factor values directly. Other materials (7075-T6 aluminum alloy, aluminum alloy, 2017-T3 aluminum alloy) used the values for initial growth

crack and nongrowth crack. For the later ones, predictions going through between the two sets of data points indicate good approximation, since the actual threshold stress intensity factor values fall between the values of initial growth crack and nongrowth crack. As shown in Fig. 5, the predicted values agree with experimental observations very well.

Theoretical s values for the MTS, the minimum strain energy density and the maximum strain energy release rate methods are 0.87, 0.96 (plane strain) and 1, respectively, regardless of the material. When the

Table 3
Experimental crack growth rate data used for model validation

Material name	References	Loading case	Mode mixity ϕ (deg)
3.5NiCrMoV forging steel	[39]	I + III	0, 30, 60
Rail steel	[40]	I + II	0, 12, 30, 65
Metal X	[41]	I + II	0, 45, 60
304 Stainless steel	[42]	I + II	0, 15, 45, 75

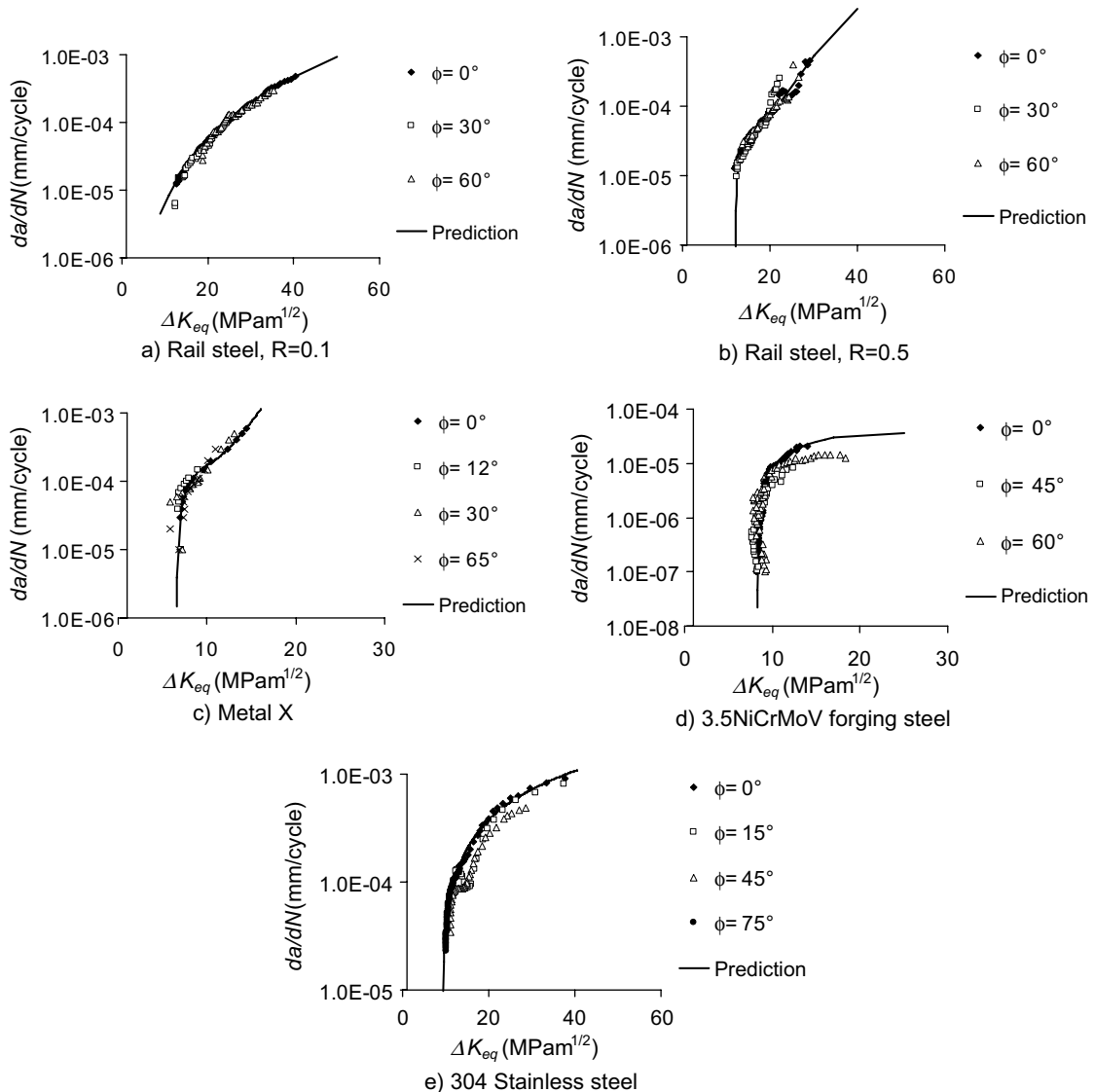


Fig. 6. Comparisons of predicted and experimental fatigue crack growth rates.

material has an s value near one of the above numbers, the corresponding model gives a reasonable prediction (see Fig. 5(d) for aluminum alloy and Fig. 5(e) for 2017-T3 aluminum alloy. The actually observed s values for the material are shown in the figures). For materials with other s values, it is seen the above three models give poor predictions (see Fig. 5(a)–(c), (f)–(h)). The proposed method generally gives better predictions than the existing three models.

3.2. Comparisons of fatigue crack growth rates

Four sets of fatigue experimental data are employed in this section, and are listed in Table 3. The predicted crack growth rates and experimental observations are plotted in Fig. 6. In Fig. 6, the x -axis is the equivalent applied stress intensity range (Eq. (11)) under mixed-mode loading. The y -axis is the fatigue crack growth rate. Different types of mixed-mode loading are represented using an angle φ , as listed in the legends for Fig. 6(a)–(e). The angle φ is defined as

$$\varphi = \tan \left(\frac{K_I}{K_{II}} \right) \quad (17)$$

As shown in Fig. 5, the proposed model correlates different types of mixed-mode crack growth rates using the mode I crack growth function. It needs to be pointed out that the proposed model is not tied to a specific function format to represent the experimental data. Instead of using the commonly used Paris law or other model forms, the best regression model form is used to represent the experimental mode I data and to predict the crack growth rate under mixed-mode loading.

4. Discussions

4.1. Crack growth under different failure mechanism

One of the advantages of the proposed model is that it can automatically adapt for different failure mechanisms, namely shear-dominated failure and tension-dominated failure. From Table 1, it can be seen that the critical plane in the proposed model depends on the material property s . It has been shown that s , the ratio of shear strength coefficient and tensile strength coefficient, is related to the material ductility [27] and to the material failure modes [6]. Once the s value is known, the proposed model can be used to predict the crack growth for any failure mechanism.

One typical observation of mixed-mode crack growth is that the underlying failure mechanism might change at different stages. Gao et al. [22] observed that fatigue crack initially propagates in a shear-mode. After growing a few grain diameters, a tensile-mode growth was observed and continued until failure. A schematic plot of the fatigue crack growth is shown in Fig. 7(a). It is well known that the total fatigue crack growth regime can be divided into three sub-regimes: near-threshold crack growth, Paris law crack growth and rapid crack growth, as shown schematically in Fig. 7(b) [43]. Gao's observations [22] indicate that both the fatigue crack growth rates and the underlying mechanisms are quite different for near-threshold crack growth and Paris law crack growth. It can be expected that tensile failure mechanism-based model and shear failure mechanism-based model cannot be applied to the entire regime of this material [22], as the cracking observation violates the physical basis of the model.

However, the proposed model can easily adapt for different failure modes, and thus is capable of representing both near-threshold crack growth and Paris law crack growth. Gao's [22] experimental observations for shear-mode and tensile-mode crack growth thresholds are plotted in Fig. 7(c). The predictions using the proposed model are also plotted. It is observed that the proposed model works well for both failure modes, i.e., $s = 0.7$ (shear dominated) and $s = 1.6$ (tension dominated).

4.2. Fatigue crack growth under nonproportional loading

For multiaxial fatigue or mixed-mode fatigue crack problem, the nonproportionality of the applied loading affects the final fatigue damage. Models based on the applied loading amplitude alone cannot capture the

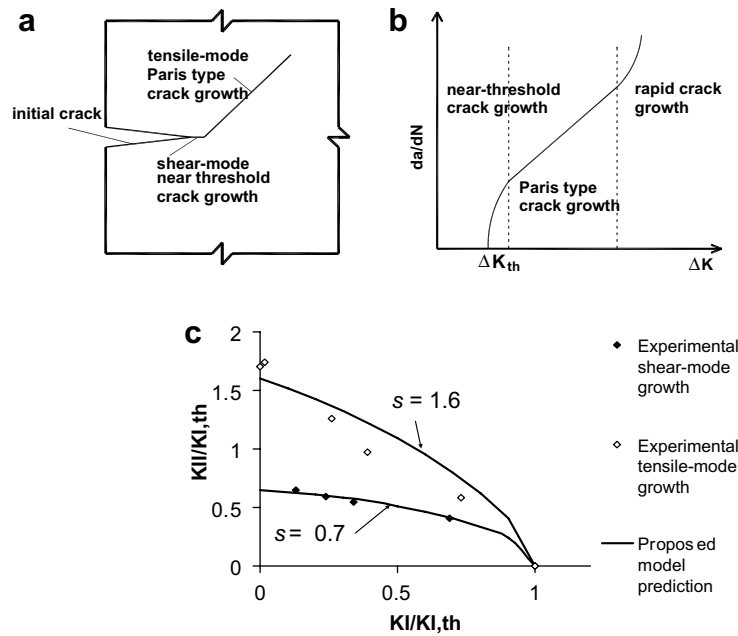


Fig. 7. Illustration of fatigue crack growth of different failure modes. (a) Schematic representation of crack growth from shear-mode to tensile-mode, (b) schematic representation of crack growth of different regimes, (c) shear-mode and tensile-mode threshold stress intensity factor stress intensity factor of 316 stainless steel.

loading path effect. The proposed model is developed from a critical plane-based model, which considers the loading path effect. In the proposed model, the critical plane depends on the maximum normal stress amplitude plane during the cyclic loading. For loadings with identical amplitudes but different loading paths, the maximum stress amplitude planes are different. Thus the fatigue damage prediction is also different.

Feng et al. [26] performed fatigue crack growth experiments under nonproportional loading and observed different crack behavior, using a nonstandard experimental set up (i.e., combined tension and torsion on a disk-shape compact tension specimen). The fatigue crack in the experiment showed complex nonplanar behavior (i.e., both branch and slant of the crack surface). The mode mixity of cracks is very complicated due to loading mixity and nonplanar crack orientation. A quantitative comparison of the proposed model with their experimental observations requires sophisticated 3D finite element analysis and crack growth analysis. That is beyond the scope of the current study. Thus, only a qualitative comparison is shown here by using a numerical example similar to the load paths used in Feng et al. [26].

The numerical example is a mixed-mode I + III crack in an infinite plate. The half-crack length is 5 mm. The load paths of remote stresses are plotted in Fig. 8. Three different load paths similar to those used by Feng et al. [26] are used. The normal stress amplitude and shear stress amplitude are assumed to be 120 MPa and 80 MPa, respectively. The stress ratio is 0.1. The material parameter s is assumed to be 0.95, which indicates brittle material property [44]. The calculation results of the critical plane orientation and stress components on the critical plane are listed in Table 4. The experimental observations by Feng et al. [26] of the crack slant angles are also listed. In order to show the crack growth rates under different load paths, the Walker equation [45] for material fatigue crack growth function is used for illustration purposes (Eq. (18)).

$$\frac{da}{dN} = \frac{3 \times 10^{-11} (\Delta K)^3}{(1 - R)^{0.5}} \quad (18)$$

where R is the stress ratio.

The crack length vs. number of cycles is plotted in Fig. 9. It is observed that the crack growth rate of path I is faster than that of path II. The stress components listed in Table 4 show that path II has smaller mean stress

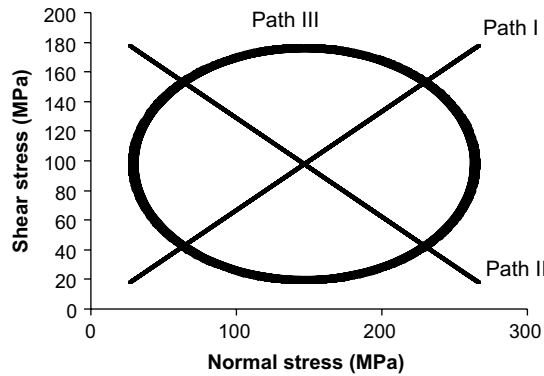


Fig. 8. Three different load paths used in the numerical example.

Table 4
Stress components on the critical plane, and critical plane orientation

Load path	$\sigma_{c,a}$ (MPa) ^a	$\sigma_{c,m}$ (MPa) ^a	$\theta_{c,n}$ (deg) ^b	$\theta_{c,e}$ (deg) ^b
Path I	144	176	43	45 (max)
Path II	144	105	43	30–60
Path III	119	188	16	8 (average)–15 (max)

^a $\sigma_{c,a}$ and $\sigma_{c,m}$ are the normal stress amplitude and mean normal stress on the critical plane, respectively.

^b $\theta_{c,n}$ is the critical plane orientation in the numerical example. $\theta_{c,e}$ is the crack slant angle from the experimental observations by Feng et al. [26].

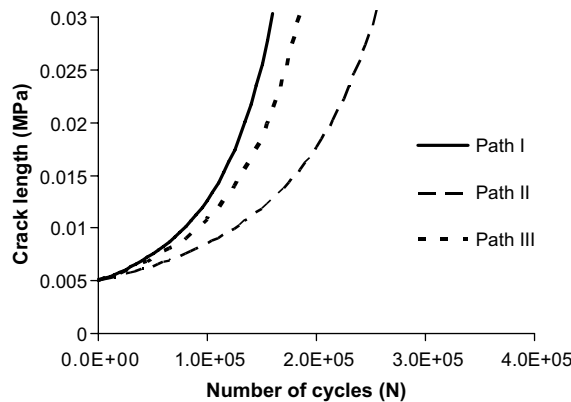


Fig. 9. Numerical predictions of crack length for the three load paths.

compared with path I. It is expected that path II will have slower crack growth rates. This numerical prediction qualitatively agrees with the experimental observations of Feng et al. [26]. However, the nonproportional load path III has a slightly slower crack growth rate compared to that of the proportional load path I. This observation is different from that of Feng et al. [26], which shows faster crack growth rate under the nonproportional load path. It is well known that nonproportional loading results in longer fatigue life in high cycle fatigue (i.e., elastic material response) compared to proportional loading with the same amplitude [46]. The reason is that proportional loading results in higher stress amplitude within the material. However, in low cycle fatigue (i.e., elasto-plastic material response), nonproportional loading results in shorter fatigue life compared to proportional loading with the same amplitude. This is due to the out-of-phase hardening effect [25]. The plastic deformation near the crack tip might be one of the reasons for the faster nonproportional crack

growth. The proposed method is a stress-based critical plane approach and does not consider plastic deformation. A strain-based critical plane approach [6] can consider plastic deformation but needs further study.

Liu and Mahadevan [6,27] have shown that the proposed concept accurately predicts the loading path effect for fatigue limit prediction, which is the same as threshold stress intensity factor predictions following the assumption of the Kitagawa diagram. Further theoretical and experimental study is needed for fatigue crack growth under general nonproportional loading and for complex mechanical components.

5. Conclusion

A new threshold stress intensity factor under mixed-mode loading is developed in this paper. The prediction based on the proposed criterion shows excellent agreement with the experimental threshold stress intensity factor data reported in the literature. The new threshold stress intensity factor criterion is then extended to develop a fatigue crack growth rate prediction model. Four sets of experimental fatigue life data under mixed-mode loading conditions are used to validate the proposed methodology. A very good agreement is obtained between experimental and predicted fatigue crack growth rates.

The proposed fatigue crack growth model is a nominal approach, which is developed using the remote stress components and the critical plane concept. Most of the existing fatigue crack growth models can only be applied to individual failure modes, i.e., shear dominated failure or tension dominated failure. Their applicability generally depends on the material's properties and loading conditions. In the proposed model, the critical plane changes corresponding to different material failure modes, thus helping the proposed model to have a wide range of applicability.

The proposed model is also capable of handling nonproportional mixed-mode loading. Compared with many of the existing fatigue crack growth models, which give identical predictions for the experiments with same amplitudes but different loading paths, the proposed model gives different predictions. However, further experimental work is required to validate the proposed methodology.

The proposed approach uses the nominal remote stress quantities. Models based on the remote stress and strain will need to be modified in order to include the overload effect and the notch effect. At present, the proposed model is applicable to mixed-mode constant amplitude loading. Further work is needed to extend the proposed model to general mixed-mode random loading.

Acknowledgements

The research reported in this paper was supported by funds from Union Pacific Railroad and Meridian Railroad (Research Agreement No. 18140, Monitor: Rex Beck). The support is gratefully acknowledged. The authors appreciate the help from Liming Liu, graduate student at Vanderbilt, in data collection.

References

- [1] Plank R, Kuhn G. Fatigue crack propagation under non-proportional mixed-mode loading. *Engng Fract Mech* 1999;62:203–29.
- [2] You BR, Lee SB. A critical review on multiaxial fatigue assessments of metals. *Int J Fatigue* 1996;18(4):235–44.
- [3] Papadopoulos IV, Davoli P, Gorla C, Filippini M, Bernasconi A. A comparative study of multiaxial high-cycle fatigue criteria for metals. *Int J Fatigue* 1997;19(3):219–35.
- [4] Bold PE, Brown MW, Allen RJ. A review of fatigue crack growth in steels under mixed-mode I and II loading. *Fatigue Fract Engng Mater Struct* 1992;15:965–77.
- [5] Qian J, Fatemi A. Mixed-mode fatigue crack growth: a literature survey. *Engng Fract Mech* 1996;55:969–90.
- [6] Liu Y, Mahadevan S. Stain based multiaxial fatigue damage modeling. *Fatigue Fract Engng Mater Struct* 2005;28:1177–89.
- [7] Varvani-Farahani A. A new energy critical plane parameter for fatigue life assessment of various metallic materials subjected to in-phase and out-of-phase multiaxial fatigue loading conditions. *Int J Fatigue* 2000;22:295–305.
- [8] Kim KS, Nam KM, Kwak GJ, Hwang SM. A fatigue life model for 5% chrome work roll steel under multiaxial loading. *Int J Fatigue* 2004;26:683–9.
- [9] Jiang Y. A fatigue criterion for general multiaxial loading. *Fatigue Fract Engng Mater Struct* 2000;23:19–32.
- [10] Jiang Y, Feng M. Modeling of fatigue crack propagation. *ASME J Engng Mater Technol* 2004;126:77–86.
- [11] Feng M, Ding F, Jiang Y. A study of crack growth retardation due to artificially induced crack surface contact. *Int J Fatigue* 2005;27:1319–27.

- [12] Erdogan F, Sih GC. On the crack extension in plates under plane loading and transverse shear. *J Basic Engng* 1963;85:519–27.
- [13] Chambers AC, Hyde TH, Webster JJ. Mixed-mode fatigue crack growth at 550 °C under plane stress conditions in Jethete M152. *Engng Fract Mech* 1991;39:603–19.
- [14] Yan X, Zhang Z, Du S. Mixed-mode fracture criteria for the materials with different yield strengths in tension and compression. *Engng Fract Mech* 1992;42:109–16.
- [15] Forth SC, Favrow LH, Keat WD, Newman JA. Three-dimensional mixed-mode fatigue crack growth in a functionally graded titanium alloy. *Engng Fract Mech* 2003;70:2175–85.
- [16] Sih GC, Barthelemy BM. Mixed-mode fatigue crack growth predictions. *Engng Fract Mech* 1980;13:439–51.
- [17] Theocaris PS, Andrianopoulos NP. The T-criterion applied to ductile fracture. *Int J Fract* 1982;20:125–30.
- [18] Chao YJ, Liu S. On the failure of cracks under mixed-mode loads. *Int J Fract* 1997;87:201–23.
- [19] Otsuka A, Mori K, Miyata T. The condition of fatigue crack growth in mixed-mode condition. *Engng Fract Mech* 1975;7:429–39.
- [20] Socie DF, Hua CT, Worthem DW. Mixed-mode small crack growth. *Fatigue Fract Engng Mater Struct* 1987;10:1–16.
- [21] Reddy SC, Fatemi A. Small crack growth in multiaxial fatigue. In: Mitchell MR, Landgraf RW, editors. *Advances in fatigue lifetime predictive techniques*. ASTM STP, vol. 1122. Philadelphia, PA: American Society for Testing and Materials; 1992. p. 276–98.
- [22] Gao H, Brown MW, Miller KJ. Mixed-mode threshold stress intensity factors. *Fatigue Fract Engng Mater Struct* 1982;5(1):1–17.
- [23] Itoh T, Sakane M, Ohnami M, Socie DF. Nonproportional low cycle fatigue criterion for type 304 stainless steel. *J Engng Mater Technol Trans ASME* 1995;117:285–92.
- [24] Borodii MV, Kucher NK, Strizhalo VA. Development of a constitutive model for biaxial low-cycle fatigue. *Fatigue Fract Engng Mater Struct* 1996;19:69–1179.
- [25] Socie D, Marquis G, editors. *Multiaxial fatigue*. Society of Automotive Engineers; 2000.
- [26] Feng M, Ding F, Jiang Y. A study of loading path influence on fatigue crack growth under combined loading. *Int J Fatigue* 2006;28:19–27.
- [27] Liu Y, Mahadevan S. Multiaxial high-cycle fatigue criterion and life prediction for metals. *Int J Fatigue* 2005;27(7):790–800.
- [28] Kitagawa H, Takahashi S. Applicability of fracture mechanics to very small cracks or cracks in early stage. In: *Proceedings of second international conference on mechanical behavior of materials*. Metal Park, OH, USA: ASM International; 1976. p. 627–31.
- [29] Liu Y, Mahadevan S. A unified multiaxial fatigue model for isotropic and anisotropic materials. *Int J Fatigue*, in press.
- [30] Liu Y, Stratman B, Mahadevan S. Fatigue crack initiation life prediction of railroad wheels. *Int J Fatigue* 2006;28(7):747–56.
- [31] Lawson L, Chen EY, Meshii M. Near-threshold fatigue: a review. *Int J Fatigue* 1999;21:15–34.
- [32] El Haddad MH, Topper TH, Smith KN. Prediction of nonpropagating cracks. *Engng Fract Mech* 1979;11:573–84.
- [33] Cotterell B, Rice JR. Slightly curved or kinked cracks. *Int J Fract* 1980;16:155–69.
- [34] Wang DZ, Ye F, Liu J, Yao CK, Wang ZG, Yu WC. Fatigue crack propagation of extruded 19V–SiCw/6061Al composite under mixed-mode (I + II) loading. *Scripta Metall Mater* 1995;32:1637–42.
- [35] Otsuka A, Tohgo K. Fatigue crack initiation and growth under mixed-mode loading in aluminum alloys 2017-T3 and 7075-T6. *Engng Fract Mech* 1987;28:721–32.
- [36] Soh AK, Bian LC. Mixed-mode fatigue crack growth criteria. *Int J Fatigue* 2001;23:427–39.
- [37] Pook LP. The fatigue crack direction and threshold behavior of mild steel under mixed-mode I and III loading. *Int J Fatigue* 1985;7:21–30.
- [38] Liu P, Wang Z. Mixed-mode I and II threshold stress intensity factor and crack deflection angle in SiCp/2024Al composite. *Scripta Mater* 1996;34(8):1323–30.
- [39] Yates JR, Mohammed RA. The determination of fatigue crack propagation rates under mixed-mode (I + III) loading. *Int J Fatigue* 1996;18:197–203.
- [40] Kim JK, Kim CS. Fatigue crack growth behavior of rail steel under mode I and mixed-mode loading. *Mater Sci Engng A* 2002;338:191–201.
- [41] Toshimitsu A, Yokobori J, Yokobori T, Sato K, Syoji K. Fatigue crack growth under mixed-modes I and II. *Fatigue Fract Engng Mater Struct* 1985;8:315–25.
- [42] Biner S. Fatigue crack growth studies under mixed-mode loading. *Int J Fatigue* 2001;23:259–63.
- [43] Suresh S. *Fatigue of materials*. 2nd ed. Cambridge University press; 1998.
- [44] Carpinteri A, Spagnoli A. Multiaxial high-cycle fatigue criterion for hard metals. *Int J Fatigue* 2001;23:135–45.
- [45] Walker K. The effect of stress ratio during crack propagation and fatigue for 2024-T3 and 7075-T6 aluminum. *ASTM STP*, vol. 462. Philadelphia: American Society for Testing and Materials; 1970. p. 1.
- [46] Socie D. Multiaxial fatigue damage models. *J Engng Mater Technol* 1987;109:293–8.